A Task Performance-Based sEMG-Driven Variable Stiffness Control Strategy for Upper Limb Bilateral Rehabilitation System

Ziyi Yang, *Student Member, IEEE*, Shuxiang Guo, *Fellow, IEEE*, Yi Liu, *Member, IEEE*, Masahiko Kawanishi, and Hideyuki Hirata

***Abstract*—Bilateral rehabilitation robotics can allow hemiplegia patients to regain the cooperative capabilities of both arms by synchronized coordination movements. Furthermore, the variable stiffness actuators (VSA) integrated robotics can offer compliant advantages for human-robot interaction. Although various studies have proposed to improve training safety and comfortability by VSA, few studies have focused on inducing patient active participation by VSA-based variable stiffness control for bilateral rehabilitation. In this article, an surface electromyography (sEMG) driven variable stiffness control framework with a novel training task quantitative factor TPI was proposed to promote patient active participation in upper limb bilateral rehabilitation. The proposed control law integrates an sEMG-driven musculoskeletal model for providing real-time dynamic reference stiffness from the nonparetic limb as a task skill learning guide to the affected limb. Furthermore, the proposed TPI is designed in the high-level controller for rendering smooth and automatic transition among three patient-robot interaction modes for inducing active participants. In the low-level controller, a position-based bilateral impedance control and a cascaded backstepping position control were implemented for compliant task position planning and tracking. Preliminary experimental results show that the proposed method can promote patient active participation by providing minimal intervention assistance for facilitating efficient upper limb rehabilitation.**

***Index Terms*—Bilateral rehabilitation, compliant physical human-robot interaction (pHRI), electromyography (EMG), task performance index (TPI), variable stiffness actuator (VSA).**

Manuscript received 29 March 2022; revised 26 July 2022; accepted 18 September 2022. Date of publication 30 September 2022; date of current version 18 April 2023. Recommended by Technical Editor S. Foong. This work was supported in part by National High Tech. Research and Development Program of China under Grant 2015AA043202, and in part by SPS KAKENHI under Grant 15K2120. *(Corresponding author: Shuxiang Guo.)*

This work involved human subjects or animals in its research. Approval of all ethical and experimental procedures and protocols was granted by the Institutional Review Board in the Faculty of Engineering, Kagawa University under Application No. 01-011.

Ziyi Yang is with the Graduate School of Engineering, Kagawa University, Takamatsu 761-0396, Japan (e-mail: zycristiano7@gmail.com).

Shuxiang Guo is with the Key Laboratory of Convergence Medical Engineering System and Healthcare Technology, the Ministry of Industry and Information Technology, Beijing Institute of Technology, Beijing 100081, China, and also with the Department of Intelligent Mechanical Systems Engineering, Kagawa University, Takamatsu 761-0396, Japan (e-mail: guo.shuxiang@kagawa-u.ac.jp).

Yi Liu is with the National Rehabilitation Center for Persons with Disabilities, Tokorozawa 359-8555, Japan (e-mail: s18d504@stu.kagawa-u.ac.jp).

Masahiko Kawanishi is with the Department of Neurological Surgery, Faculty of Medicine, Kagawa University, Takamatsu 761-0793, Japan (e-mail: mk@kms.ac.jp).

Hideyuki Hirata is with the Faculty of Engineering and Design, Kagawa University, Takamatsu 761-0396, Japan (e-mail: hirata.hideyuki@kagawa-u.ac.jp).

Color versions of one or more figures in this article are available at https://doi.org/10.1109/TMECH.2022.3208610.

Digital Object Identifier 10.1109/TMECH.2022.3208610

I. Introduction

FOR hemiplegia patients, the bilateral rehabilitation strategy is considered a promising approach to promote neuroplasticity and natural inter-limb coordination [1]. As one side functional disability of hemiplegia, the dynamic motion information of the nonparetic limb could be utilized as a reference guide for the affected limb to perform the predefined coordination training in bilateral rehabilitation [2], [3]. Accordingly, the rehabilitation robotics systems, including exoskeleton type [4], [5], [6], [7], fixed planar platform type [8], parallel robot type [9], and end-effector type [10], have been developed for upper limb bilateral rehabilitation [11].

To avoid the secondary injury caused by the conflict of patient-robot interaction [12], compliance actuators have been integrated into rehabilitation robotics, such as series elastic actuators [13] and variable stiffness actuators (VSA) [14], [15]. Especially to VSA [14], unlike rigid robots, the VSA-integrated robotics can render the passive-compliance to the physical human-robot interaction (pHRI) and are robust to external disturbance and adaptable for precision force interaction with humans to achieve safer pHRI [16], [17]. In addition, compliance control is widely applied within the compliant robotic system, as it can balance the human active efforts to perform the desired compliance characteristics for the safe pHRI. In our previous works, some rehabilitation robotics systems [18], [19] involving myoelectric control or haptic control have been developed for improving bilateral rehabilitation effects [20], [21]. Furthermore, we proposed a novel home-based powered variable stiffness exoskeleton device (PVSED) which is adaptive to patients' dynamic movements for improving the training comfortability and safety [22], [23].

Not only the patient training safety, but the patient recovery effect is also the other critical research point of robotic-assisted

1083-4435 © 2022 IEEE. Personal use is permitted, but republication/redistribution requires IEEE permission.
See https://www.ieee.org/publications/rights/index.html for more information.

Authorized licensed use limited to: NANKAI UNIVERSITY. Downloaded on April 19,2023 at 02:19:00 UTC from IEEE Xplore. Restrictions apply.

rehabilitation [24]. How much and when the robotic assistance should be delivered to the patients for better recovery effect remains an open problem [25]. As active participation can induce neural plasticity [26], the control strategy of rehabilitation robots should have the ability to promote active participation [27]. That requires the robotics can provide the necessary minimal assistance to patients to complete the training task, which is also well-known as the paradigm of assist-as-needed (AAN) [28], [29], [30], [31], [32]. In the patient-robot interaction of VSA-integrated robots, the patient active voluntary can be measured by a surface electromyography (sEMG) driven model [33] or some control method such as inverse dynamic [34] and observer [35]. The training task performance is considered a key metric to assess patient active participation [35], [36], [37]. Therefore, the proportion of pHRI should be adaptively regulated according to the task performance for achieving AAN policy [38], [39], [40], [41], [42], [43].

As the aforementioned discussion, there are various researches have made progress in improving the safety of pHRI using compliant robotics and promoting patient active participation. However, few studies have focused on inducing active participation in patient-robot interaction of the VSA-integrated robotics for bilateral rehabilitation training tasks. For biofeedback signal implementation, some studies involved the EMG signals for human active torque estimation rather than implementing it into the control framework [34]. In addition, although the compliant control strategies of VSA-integrated robotics have been achieved by force sensors, relatively few works have been reported for position-based compliant control framework of VSA-integrated robotics to avoid force sensor position sliding during patient-robot interaction. Furthermore, the rehabilitation task performance is usually described by position tracking error or toque, which may lack comprehensive analysis of different task intensities. Therefore, motivated by the above-introduced studies, we argue that the VSA-integrated rehabilitation robotics not only can improve the safety of pHRI, but also have the potential on promoting patient active participation.

In this article, we presented an sEMG-driven variable stiffness control strategy based on the task performance for inducing patient active participation in bilateral training rehabilitation. In this concept (see Fig. 1), the proposed stiffness control framework utilizes the sEMG signals and elbow angle on the contralateral side as the guidance to regulate the desired stiffness and trajectory. The stiffness can be smoothly regulated among patient-in-charge mode, patient-robot cooperation mode, and robot-in-charge mode according to the sEMG-driven task performance index (TPI). The compliant position is planned by a position-based bilateral impedance control and tracked by the backstepping approach-based position controller of VSA. To the best of our knowledge, this is the first work focused on inducing patients' active participation using the task performance-based stiffness control of VSA-integrated robotic for bilateral rehabilitation. The main contributions are summarized as follows:

1) The proposed variable stiffness control strategy can realize the autosmooth transition of multistiffness-modes to adaptively adjust the assistance level for achieving AAN policy, which is driven by a novel task performance quantitative factor TPI designed with training skills and biofeedback signals.
2) A position-based compliant control framework of VSA, including position-based bilateral impedance control and backstepping approach-based position control, was proposed to realize the force-sensorless tracking control under the TPI-driven stiffness control law.
3) The impedance characteristics of dynamic task motions from the contralateral side limb can be adaptively transferred to the affected side by TPI for rendering human-like behavior patterns and specific task skills of bilateral training.

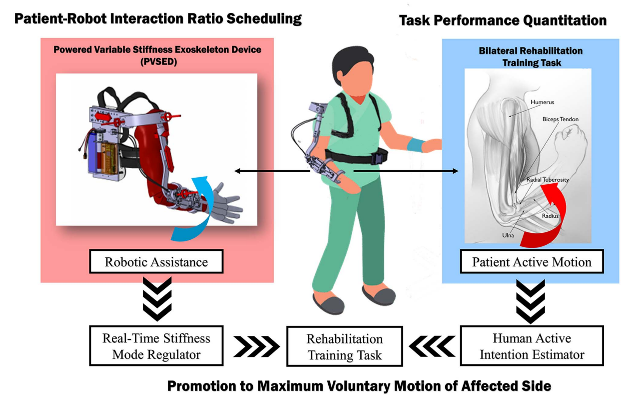

Fig. 1. Concept of task performance-based sEMG-driven variable stiffness control strategy in bilateral rehabilitation for inducing patients' active participations.

This article is organized as follows: in Section II, the mechanical design and dynamics of the PVSED will be introduced for human active torque estimation. In Section III, the sEMG-driven musculoskeletal model would be reviewed for obtaining real-time dynamic reference stiffness from the nonparetic limb as coordinated bilateral motor skill learning guidance for the affected limb. Then, the performance-based control law including TPI and three stiffness modes of the high-level controller (HLCL) and position-based impedance control with a cascaded backstepping position control as the low-level controller (LLCL) will be presented in Section IV. The evaluation experiments of the proposed control framework were introduced in Section V and discussed in Section VI. Finally, the conclusion is drawn in Section VII.

II. Hardware Description and Dynamics

A. Mechanical Structure of PVSED

The PVSED was designed in a lightweight, comfortable, and wearable structure for high portability, as shown in Fig. 2(a). The mechanical design and the kinematic analysis of the PVSED were detailly introduced in our previous research [21]. The PVSED is capable of independently actuating the patients' flexion/extension (FE) of the elbow joint and joint stiffness variation through a main joint actuation system and an independent-setup VSA system. The main joint actuation system can provide the joint torque on the pulley to drive the mainframe through a

Authorized licensed use limited to: NANKAI UNIVERSITY. Downloaded on April 19,2023 at 02:19:00 UTC from IEEE Xplore. Restrictions apply.

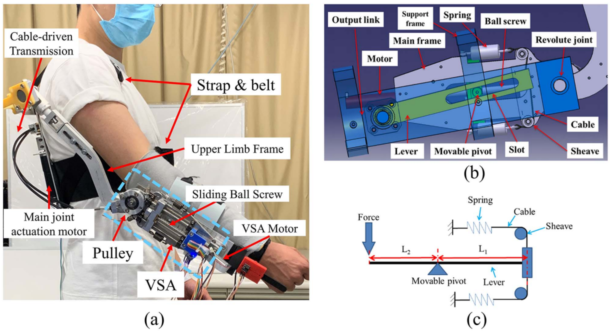

Fig. 2. Mechanical design of the PVSED. (a) Components of the PVSED. (b) Schematic of the VSA. The pivot can be moved along the lever to adjust the transmission ratio between the spring and the exerted force. (c) Dynamic model of the PVSED.

cable-driven transmission mechanism by a compact DC motor M_1 (Maxon RE-30 Graphite Brushes Motor). The VSA system is assembled into the mainframe part of the PVSED coupled with the output link by the pully and lever with a pair of antagonistic springs, as shown in Fig. 2(b) and (c). As the leverage of the elastic force of the antagonistic springs of the VSA system, the output torque of the elbow joint will be delivered from the mainframe to the output link to assist the patient's movements. Additionally, the pivot of the VSA can be driven by a small-size DC motor M_2 (Maxon RE-13 Graphite Brushes Motor) through the ball screw transmission along with the slot in the output link lever to realize the change of the lever ratio between the output lever and the elastic elements lever for realizing variable stiffness adjustment. Thus, the variable stiffness of the output link can be determined by adjusting the pivot position. As verified in our previous study [22], the relationship between the pivot position and output stiffness can be described as following by using a second-order polynomial curve fitting method

$$K(\theta_2) = 16.55L_p(\theta_2) + L_p(\theta_2) + 16.95 \tag{1}$$

where K is the stiffness of the PVSED and θ_2 represents the rotation angle of RE-13 motor of VSA and $L_p(\theta_2)$ refers to the pivot position. The stiffness of the PVSED can be adjusted as a reference dynamic stiffness profile to provide compliant assistant and motor learning guidance to the patients by converting the rotary motion of a slide screw to the linear motion of the pivot assembly.

B. PVSED Dynamics

For the rehabilitation scenarios in which the robots closely interact with patients, the dynamic interaction should be considered for the safety and comfortability of the patient. The dynamics of the 1-Dof PVSED in consideration of the human-robot interaction can be described as follows:

$$J_j\ddot{\theta}_j + B_j\dot{\theta}_j + G_j = \tau_j + \tau_h \tag{2}$$

$$J_1\ddot{\theta}_1 + B_1\dot{\theta}_1 + \tau_j/\gamma_1 = \tau_1 \tag{3}$$

$$J_2\ddot{\theta}_2 + B_2\dot{\theta}_2 + \tau_s/\gamma_2 = \tau_2 \tag{4}$$

$$\tau_j = K(\theta_2)(\theta_1 - \theta_j) \tag{5}$$

where θ_j, θ_1, and θ_2 are the angle position of the output link, main actuation system motor M_1 (RE-30), and VSA system motor M_2 (RE-13), respectively. Accordingly, the $\dot{\theta}_j$, $\dot{\theta}_1$, $\dot{\theta}_2$ denote the angular velocity, and $\ddot{\theta}_j$, $\ddot{\theta}_1$, $\ddot{\theta}_2$ represent angular acceleration. The complexed human forearm and the PVSED is shown as the (2), the τ_j is the VSA output torque applied to the joint and the τ_h denotes the human active torque. J_J, B_J, and G_J represent the inertia, damping, and gravitational torque, respectively. As the independent VSA working principle, the τ_j can be calculated as (5). The J_{i} stands for the motor inertia and B_{i} is the motor damping coefficient, where $i = 12$ represents the motor M_1 and M_2. Moreover, the γ_1 and γ_2 are the transmission ratios of the main actuation system and the VSA system. The main actuation system and the VSA system can be described using (3) and (4) The τ_s reveals the resistance force generated by the elastic deflection during the variable stiffness.

C. Sensorless Human Active Torque Estimation

Due to the force collection would be affected caused by relative sliding between the exoskeleton and the human arms, the compliant actuators become a suitable solution to estimate the interaction force by converting the force measurement problem into a deflection position measurement problem. In this article, the inverse dynamics of the PVSED considering the human-robot interaction were utilized to estimate the human active torque

$$\hat{\tau}_h = J_j\ddot{\theta}_j + B_j\dot{\theta}_j + G_j - K(\theta_2)(\theta_j - \theta_1) \tag{6}$$

where the $\hat{\tau}_h$ denotes the estimated human active torque interacted with the PVSED. And the angular acceleration $\ddot{\theta}_j$, angular velocity $\dot{\theta}_j$, and angular θ_j were measured by an inertial measurement unit (GY-25T tilt angle module) which integrated a digital motion processor for noise filtering. The $J_j = J_D + J_h$ is the total inertia of the PVSED (J_D= 0.45 kgm^2) and human forearm J_h. According to Dinh et al. [44]. The mass of the human forearm m_f and length from the center of mass of the forearm to the elbow joint l_f can be calculated by an individual's physical parameters. The m_f equals to 0.022 times human height, l_f equals to 0.682 times total forearm length, and the inertia coefficient and damping coefficient can be calculated as follows:

$$J_h = \frac{2}{3}m_f \cdot l_f^2 \tag{7}$$

$$B_j = 2J_h\omega\xi,\ \omega = \sqrt{\frac{mgl_f}{J_h}},\ \xi = 0.7. \tag{8}$$

Therefore, the J_h can be derived by $J_h = \frac{2}{3}m_f\ l_f^2$ for simply, so that is 0.08 kgm^2, and $J_j = J_D + J_h$ is 0.53 kgm^2. Then, B_j is 0.24 Nm/rad by (8). $G_j = m_f\, g\sin(\theta_j)$, where $g = 9.81$ m/s^2.

III. sEMG-Driven Musculoskeletal Model

A. sEMG Signals Collection and Muscle Activation

The sEMG signals generated from the center neural system can activate the muscle fiber's contraction motion by neural impulses. The muscle activation dynamic can be calculated from

Authorized licensed use limited to: NANKAI UNIVERSITY. Downloaded on April 19,2023 at 02:19:00 UTC from IEEE Xplore. Restrictions apply.

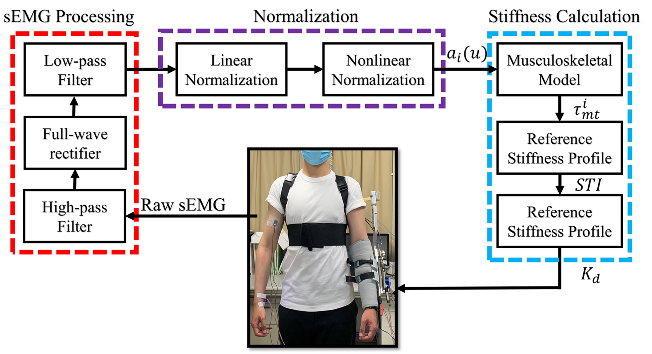

Fig. 3. EMG signals processing procedure for real-time muscle activation and reference stiffness.

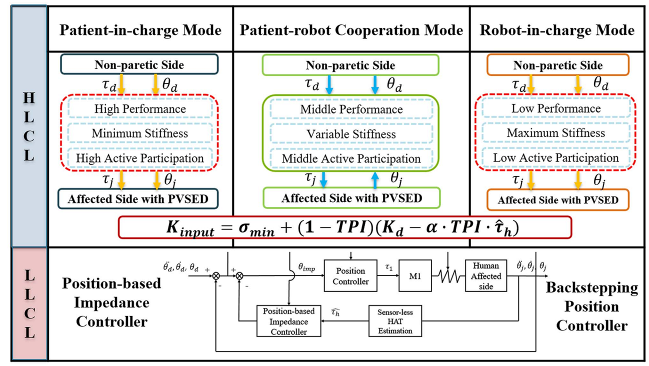

Fig. 4. sEMG-driven variable stiffness control framework based on the TPI including patient-in-charge mode, patient-robot cooperation mode and robot-in-charge mode.

sEMG signals to evaluate the muscle contraction motions. In this article, the sEMG signals were collected by the commercial EMG device (Personal-EMG, Oisaka Electronic Equipment Ltd, Japan) at a 1000 Hz sampling rate. Note that the raw sEMG signals should be preprocessed as Fig. 3 to get the muscle activation for real-time stiffness estimation. After the preprocessing, the filtered sEMG signals should be normalized by the maximum voluntary contraction test to obtain the normalization value. Finally, the muscle activation can be calculated by a nonlinear normalization as the following formula:

$$a_i\left(u\right) = \frac{e^{Au_i} - 1}{e^{u_i} - 1} \tag{9}$$

where u_i is the normalized signals of the ith muscle and the $a_i(u)$ is according to muscle activation. Furthermore, the A is the nonlinear shape factor, constrained from 0 to -3.

B. Muscle Contraction Dynamics

As the literature reported [45], the muscle contraction dynamics are generally described by the Hill-type muscle model, including an active contractile element (CE), a passive parallel elastic element (PE), and a series elastic element (SE). Elbow flexion and extension in the sagittal plane are principally accomplished by the concentric/eccentric contraction of an antagonistic muscle pair. In our previous study, we established a musculoskeletal model to describe the muscle contraction dynamics during human elbow movements. In this model, the single muscle is represented by a pair of antagonistic muscle-tendon units with bones to describe the muscle-tendon force F^{mt} for simplification as follows:

$$F_{mt}^i = F_{\mathrm{CE}}\left(a_i\left(u\right), l_{mt}^i\right) + F_{\mathrm{PE}}\left(l_{mt}^i\right) \tag{10}$$

$$l_{mt}^i = l_t^i + l_m^i \cos\phi \tag{11}$$

$$r_{mt}^i = \frac{\partial l_{mt}^i}{\partial \theta} \tag{12}$$

$$\tau_{mt}^i = F_{mt}^i \cdot r_{mt}^i \tag{13}$$

where F_{CE} presents the active contractile force, which can be obtained by muscle activation $a(u)$ and F_{PE} presents passive elastic force. l_{mt}^i and r_{mt}^i are the length and moment of the muscle-tendon. φ and θ are the negligible pennation angle of muscle-tendon and joint angle. Therefore, the elbow flexion and extension can perform by the pair of the antagonistic muscles, Biceps Brachii and Triceps Brachii (BB and TB), in which the net torque of the elbow joint is

$$\tau_{\mathrm{elbow}} = \left|\tau_{mt}^{BB}\right| - \left|\tau_{mt}^{TB}\right| = \left|F_{mt}^{BB} \cdot r_{mt}^{BB}\right| - \left|F_{mt}^{TB} \cdot r_{mt}^{TB}\right|. \tag{14}$$

Moreover, the stiffness trend index (STI) is defined as

$$\mathrm{STI} = \left|\tau_{mt}^{BB}\right| + \left|\tau_{mt}^{TB}\right|. \tag{15}$$

The stiffness of the joint is calculated as

$$K_d = \alpha \cdot \mathrm{STI} + \beta \tag{16}$$

where α (rad^{-1}) and β (N·m/rad) are the constants according to the different training tasks and individual-specific conditions ($\alpha = 10$, $\beta = 1$, in this article). Benefiting from this model, the dynamic stiffness of the human joint motor can be calculated to describe the physical properties of the elbow joint. Then, the nonparetic side joint stiffness K_d will be utilized as the reference stiffness input of the performance-based variable stiffness control to describe motor skills in different tasks during bilateral coordinated movements.

IV. Performance-Based Control Law

In this section, by incorporating the TPI in the HLCL, position-based impedance control, and cascaded backstepping position control in the LLCL within the overall control framework, an sEMG-driven variable stiffness control framework is proposed based on the task performance for bilateral rehabilitation training. The proposed stiffness control framework, shown in Fig. 4, utilizes the sEMG signals and elbow angle on the contralateral side as the guidance to regulate the desired stiffness and trajectory. The patient's non-paretic side elbow angle θ_d is selected as the position input for PVSED tracking. Meanwhile, the raw sEMG signals on this side are recorded and subsequently processed to calculate the real-time reference stiffness K_d which will be used as the stiffness profile reference. In this processing, the affected side assisted by the PVSED would be asked to complete the bilateral rehabilitation cooperation task with

Authorized licensed use limited to: NANKAI UNIVERSITY. Downloaded on April 19,2023 at 02:19:00 UTC from IEEE Xplore. Restrictions apply.

the subject maximum efforts $\hat{\tau}_h$, which will be obtain by the sensorless torque estimation method.

A. Task Performance Index

In this article, the TPI, TPI, is proposed for bilateral training that can achieve the smooth variable stiffness transition during three stiffness models based on the task performance. First, the task performance is usually evaluated by the tracking error between the contralateral side and the PVSED-assisted side by a trajectory region function. According to the individual-specific and training requirements, the trajectory region can be divided into three regions, including the patient active region, the co-operation region, and the patient passive region. The trajectory region is given as

$$h\left(\theta_e\right) = \|\theta_e\|^2 - R_a^2 \tag{17}$$

$$\theta_{\mathrm{e}} = \theta_{jr} - \theta_j \tag{18}$$

where R_a is a positive constant that represents the radius of the patient active region. The θ_{jr} is the reference position of the contralateral side limb and the θ_j stands for actual position of affected limb. When θ_e is inside the patient active region, $h(\theta_e) \leq 0$, and vice versa.

Based on the trajectory region, the TPI is defined as follows:

$$\mathrm{TPI}(h) = \frac{1}{1 + e^{a*h*K_d - R_a}} \tag{19}$$

where K_d represents the desired stiffness calculated from the sEMG signals of the contralateral side. R_a and a are the positive constants representing the radius of the trajectory region and the positive constant to satisfy the max limited stiffness variable velocity, respectively. From (19), the TPI is bounded 0<TPI<1. When trajectory tracking error θ_e is inside the patient active region, such that $\theta_e < R_a$ and $h(\theta_e) < 0$, $\mathrm{TPI}(\theta_e) \rightarrow 1$. When trajectory tracking error θ_e reaches the patient passive region, such that $\theta_e > R_p\, h(\theta_e) > 0, \mathrm{TPI}(\theta_e) \rightarrow 0$. Due to the infinitely differentiable characteristics of TPI, the transition process is smooth during $h(\theta_e)$ continuously variation.

From Fig. 5(a), the value of the TPI's inflection point is always 0.5 and locates in the middle of the patient active radius R_a and patient passive radius R_p according to the properties of (19). That means the human efforts are equal to the robot efforts at the inflection point, which is defined as the balance points of patient-robot interaction in this article. Furthermore, based on the concavity and convexity of both sides of the inflection points, the TPI transition process can be divided into two subregions, the slope increase region (SIR) and slope decrease region (SDR), shown as Fig. 5(a). In the SIR, the slope of TPI will gradually increase until to the max at balance points of patient-robot interaction, so that the patients are encouraged to correct their movements by themselves efforts of this region for minimal intervention therapy. On the contrary, the slope of TPI is progressively decreasing from the maximum value to zero along with the tracking error increasing in the patient passive region R_p in the SDR. By this property, the fast correction force can be realized by rapidly increasing stiffness, and the relatively slow speed of variable stiffness at a high stiffness level can protect patients from the

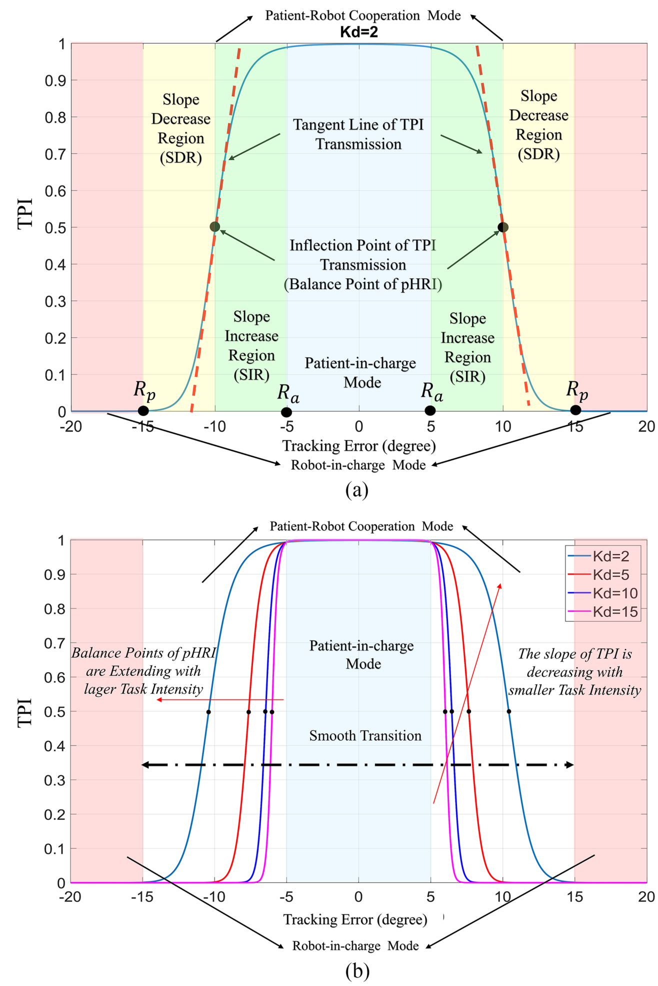

Fig. 5. Illustration of the TPI. (a) TPI-driven three stiffness modes, balance point, and slope region analysis of TPI versus K_d=2, with a=0.08, $R_a = 5°$, $R_a = 15°$. (b) Task intensity influence analysis of TPI versus K_d=25,10,15, with a=0.08, $R_a = 5°$, $R_a = 15°$.

sudden variation of high contact force to improve the safety of rehabilitation training.

In addition, task intensity is also a key metric of rehabilitation training for evaluating different injury levels and individual-specific, which can be reflected by muscle activation and stiffness. For this consideration, K_d term in (19) is designed for regulating the TPI variation rate. This property is designed to adjust the TPI parameter according to the different task intensities which can express the different influences of task intensity. The higher level of K_d can lead to faster TPI regulation and a more medial position of the balance point of patient-robot interaction, shown in Fig. 5(b).

In practice, the active radius R_a and passive radius R_p should be determined according to the individual-specific and task requirements. Then, the parameter a can be derived by $a * K_d * h\left(\frac{R_a+R_p}{2}\right) - R_a = 0$, as the inflection points of TPI are the middle points between the patient-in-charge mode and robot-in-charge mode. K_d in here, should be the minimal value for obtaining a larger adjustable range.

Authorized licensed use limited to: NANKAI UNIVERSITY. Downloaded on April 19,2023 at 02:19:00 UTC from IEEE Xplore. Restrictions apply.

B. TPI-Based Stiffness Controller for Bilateral Training

Three stiffness control modes are identified to adapt to different injury level patients, including patient-in-charge mode, patient-robot cooperation mode, and robot-in-charge mode. These three stiffness modes, which can be auto-smoothly transited by TPI, are implemented by a single stiffness controller in the HLCL. The total stiffness control input of the PVSED is given as

$$K^{\mathrm{TPI}} = \sigma_{\min} + (1 - \mathrm{TPI})\left(K_d - \mathrm{TPI}\cdot(\alpha\cdot\hat{\tau}_h + \beta)\right). \quad (20)$$

Due to the main efforts are caused by biceps rather than triceps in the bilateral lifting task, the torque of elbow τ_{elbow} can be approximates to the STI. Therefore, the musculoskeletal model and its inverse model were utilized for calculating the desired stiffness profile K_d and estimated human stiffness $\alpha\cdot\hat{\tau}_h + \beta$ in real-time. These two items are designed to reduce human active torque influence on stiffness regulation for minimal assistance. And $\sigma_{\min}$ represents the minimal mechanical inherent stiffness of the PVSED. According to the characteristics of TPI, the three stiffness modes is defined as follows:

1) Patient-in-Charge Mode: The patient-in-charge mode satisfies the high level and well-recovered hemiplegia patients in the last rehabilitation stage. When the trajectory tracking errors are lower than the predefined threshold, the patients would be considered as having the ability to perform the current training task so that the interaction stiffness should be minimal. The stiffness control input in the (20) becomes

$$K^{\mathrm{TPI}} \to \sigma_{\min}, \|\theta_e\| < R_a. \quad (21)$$

K_{input} is the minimum value among the three stiffness modes. Additionally, only if the patients try their best to perform the training task, the patient-in-charge mode could be kept, which can motivate the patient's active participation.

2) Patient-Robot Cooperation Mode: For the middle rehabilitation stage, if the patient cannot continuously perform the bilateral training tasks in the high performance but within the predefined acceptable error range R_p, the TPI will be within 0 to 1 and the patient-robot interaction mode is achieved in which the minimal assistance will be delivered to patients according to their task performance. In this mode, the control input remains the (18)

$$\begin{aligned} K^{\mathrm{TPI}} &= \sigma_{\min} + (1 - TPI)\left(K_d - TPI\cdot(\alpha\cdot\hat{\tau}_h + \beta)\right) \\ R_{\mathrm{a}} &\le \|\theta_e\| \le R_p. \end{aligned} \quad (22)$$

The adaptive position-dependent weight factor TPI can adjust the stiffness control input for regulating the proportion of pHRI. Benefiting from the SIR and SDR, compliant AAN control can be achieved.

3) Robot-in-Charge Mode: Only if poor performance appears, the robot-in-charge mode will be reached for correcting the unexpected task errors of the patient. Due to the poor performance, the TPI will equal 0 so that the real-time desired stiffness of the contralateral side limb will be directly transferred to the affected side as follows:

$$K^{\mathrm{TPI}} \to \sigma_{\min} + K_d, R_p < \|\theta_e\|. \quad (23)$$

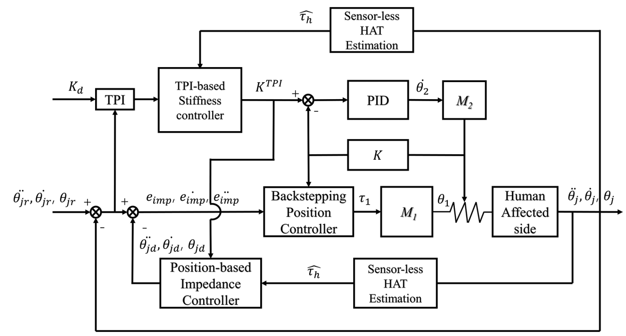

Fig. 6. Block diagram of the closed-loop system.

This mode is designed for serious hemiplegia patients so that the bilateral cooperation motor skill will be unaltered delivered to the disability-affected side limb. The patients can be benefited from this comprehensive guidance as relearning the bilateral cooperation motor skills and rebuilding the recovery confidence.

C. Position-Based Bilateral Impedance Controller

As the effects of the TPI-driven variable stiffness controller, the impedance characteristics of the system should also be dynamic to adapt to the symmetric bilateral training task according to the synchronic reference impedance of the contralateral side limb. The block diagram of overall system is shown in Fig. 6. The position-based impedance controller is given as follows:

$$M_{\mathrm{m}}\left(\ddot{\theta}_{jd} - \ddot{\theta}_j\right) + B_{\mathrm{m}}\left(\dot{\theta}_{jd} - \dot{\theta}_j\right) + K_{\mathrm{m}}\left(\theta_{jd} - \theta_j\right) = \hat{\tau}_h \quad (24)$$

$$K_{\mathrm{m}} = K^{\mathrm{TPI}} \quad (25)$$

$$B_{\mathrm{m}} = v_m\sqrt{K_m} \quad (26)$$

where the angular position θ_{jd}, angular velocity $\dot{\theta}_{jd}$ and angular acceleration $\ddot{\theta}_{jd}$ are desired compliant trajectory modified by the impedance controller. The M_m, B_m, and K_m, are the inertia, damping, and stiffness parameters of the contralateral side limb, respectively. The M_m can be obtained by (7). And the dynamic stiffness and damping of the contralateral side limb can be realized by (25) and (26), where the v_m is the damping coefficient set as 0.7. It should be noted that the suitable inertia terms and damping terms will bring energy dissipation for safe patient-robot interaction. Then, the desired compliant trajectory (θ_{jd} $\dot{\theta}_{jd}$ and $\ddot{\theta}_{jd}$) can be derived by (24) after obtaining the reference trajectory from the contralateral side limb (θ_{jr} $\dot{\theta}_{jr}$ and $\ddot{\theta}_{jr}$), actual trajectory from the affected side limb (θ_j, $\dot{\theta}_j$, and $\ddot{\theta}_j$), and estimated human active torque $\hat{\tau}_h$. Therefore, trajectory error can be calculated by $e_{\mathrm{imp}} = \theta_{jr} - \theta_{jd} - \theta_j$, $\dot{e}_{\mathrm{imp}} = \dot{\theta}_{jr} - \dot{\theta}_{jd} - \dot{\theta}_j, \ddot{e}_{\mathrm{imp}} = \ddot{\theta}_{jr} - \ddot{\theta}_{jd} - \ddot{\theta}_j$ which will be utilized as the input of the backstepping position controller. Benefited from (25) and (26), the dynamic impedance characteristic of the contralateral side limb can be rendered to the affected side by the TPI-driven variable stiffness and corresponding damping for providing human-like behavior patterns and bilateral task skill transfer.

Authorized licensed use limited to: NANKAI UNIVERSITY. Downloaded on April 19,2023 at 02:19:00 UTC from IEEE Xplore. Restrictions apply.

D. Backstepping Position Controller of PVSED

The motion tracking problem of the variable stiffness robotics usually refers to the guarantee of robotic motions can converge to the desired trajectory during the stiffness regulation process. In this article, the motion of the PVSED should track the planned position trajectory derived from the position-based bilateral impedance controller. So, the backstepping approach was selected to realize the tracking control of the PVSED. For realizing backstepping control, the (2) and (3) can be rewritten into the state-space form

$$\begin{bmatrix} \dot{z}_1 \\ \dot{z}_2 \\ \dot{z}_3 \\ \dot{z}_4 \end{bmatrix} = \begin{bmatrix} 0 & 1 & 0 & 0 \\ \frac{K^{\mathrm{TPI}} - B_j}{J_j} & \frac{-B_j}{J_j} & \frac{K^{\mathrm{TPI}}}{J_j} & 0 \\ 0 & 0 & 0 & 1 \\ \frac{-K^{\mathrm{TPI}}}{J_1\gamma_1} & 0 & \frac{K^{\mathrm{TPI}}}{J_1\gamma_1} & \frac{B_1}{J1} \end{bmatrix} \begin{bmatrix} z_1 \\ z_2 \\ z_3 \\ z_4 \end{bmatrix} + \begin{bmatrix} 0 \\ 0 \\ 0 \\ 1 \end{bmatrix} u \tag{27}$$

where $z_1 = \theta_j$, $z_2 = \dot{\theta}_j$, $z_3 = \theta_1$, $z_4 = \dot{\theta}_1$, are the state variable parameters of the state-space model. And z_{1d}, z_{2d}, z_{3d}, z_{4d}, are the desired value of the corresponding state variable parameters. To let the position of the output link can tracking the desired trajectory derived from the position-based bilateral impedance controller by the main actuator motor position θ_1 during the TPI-driven variable stiffness process, the first control law of the backstepping position controller is chosen as:

$$\theta_{1d} = \frac{J_j}{K^{\mathrm{TPI}}}\left(e + \dot{z}_{2d} + \frac{B_j}{J_j}\dot{z}_1 + \frac{G_j + K^{\mathrm{TPI}}}{J_j}z_1 + k_2\delta\right) \tag{28}$$

$$z_{2d} = \dot{z}_{1d} + k_1 e \tag{29}$$

where the control gain k_1 and k_2 both are positive definite. The errors are defined by $e = z_{1d} - z_1$, $\delta = z_{2d} - z_2$.

The second control goal of the backstepping position controller is realizing the main actuator motor tracking this desired position trajectory obtained from (28) by the motor torque. The second control law is given by

$$\tau_{1d} = m_1\left(\Upsilon + \dot{z}_{4d} - \frac{B_1}{J_1}\dot{z}_3 + \frac{K^{\mathrm{TPI}}}{J_1\gamma_1}(z_3 - z_1) + k_4\Gamma\right) \tag{30}$$

$$z_{4d} = \dot{z}_{3d} + k_3\Upsilon \tag{31}$$

where the τ_{1d} is the desired torque of the motor *M1* and the control gain k_3 and k_4 both are positive definite. The errors are defined by $\Upsilon = z_{3d} - z_3$, $\Gamma = z_{4d} - z_4$.

E. Stability Analysis

The stability of the proposed bilateral rehabilitation system under the TPI-driven variable stiffness control law can be analyzed by a Lyapunov function method. As given in Section IV-D, the tracking errors are defined as

$$e = z_{1d} - z_1, \delta = z_{2d} - z_2, \Upsilon = z_{3d} - z_3, \Gamma = z_{4d} - z_4. \tag{32}$$

Then, the Lyapunov candidate function is chosen as follows:

$$V = V_1 + V_2 + V_3 + V_4 = \frac{1}{2}e^2 + \frac{1}{2}\delta^2 + \frac{1}{2}\Upsilon^2 + \frac{1}{2}\Gamma^2 > 0. \tag{33}$$

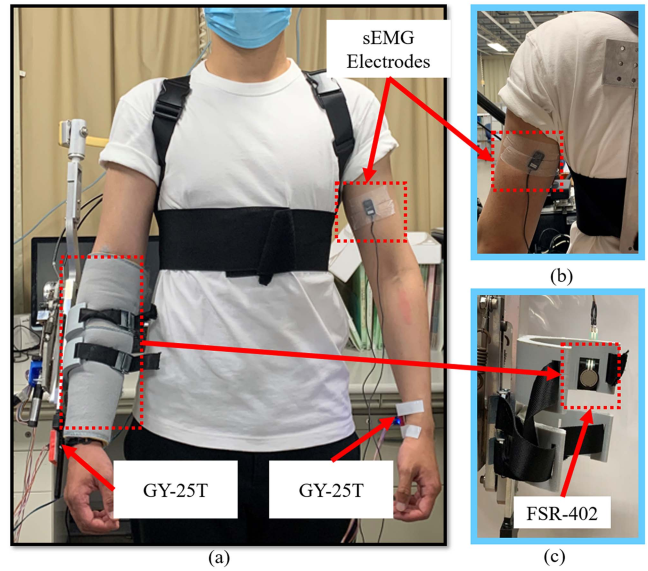

Fig. 7. Experimental setups. (a) Front view of the PVSED with a wearer. (b) Lateral view of the sEMG electrode placements. (c) Detailed view of the FSR-402 force sensor placement.

Taking the derivative of (33), which consists of four subfunctions:

$$\dot{V} = \dot{V}_1 + \dot{V}_2 + \dot{V}_3 + \dot{V}_4. \tag{34}$$

And substituting the control laws (28)–(31), the derivative of each subfunction can be obtained as

$$\dot{V}_1 = e \cdot \dot{e} = e \cdot (\dot{z}_{1d} - z_{2d} + \delta) = -k_1 \cdot e^2 + e \cdot \delta \tag{35}$$

$$\dot{V}_2 = \delta \cdot \dot{\delta} = \delta \cdot (\dot{z}_{2d} - z_2) = -k_2 \cdot \Upsilon^2 - e \cdot \delta \tag{36}$$

$$\dot{V}_3 = \Upsilon \cdot \dot{\Upsilon} = \Upsilon \cdot (\dot{z}_{3d} - z_{4d} + \Gamma) = -k_3 \cdot \Upsilon^2 + \Upsilon \cdot \Gamma \tag{37}$$

$$\dot{V}_4 = \Gamma \cdot \dot{\Gamma} = \Gamma \cdot (\dot{z}_{4d} - z_{4d} + \delta) = -k_4 \cdot \Gamma^2 - \Upsilon \cdot \Gamma. \tag{38}$$

As the characteristic of the backstepping controller, the last terms of (35), (36) and (37), (38) can be canceled by each other. Therefore, the sum of the derivatives can be given as follows:

$$\dot{V} = -k_1 e^2 - k_2\delta^2 - k_3\Upsilon^2 - k_4\Gamma^2 \leq 0. \tag{39}$$

Due to the function is negative semidefinite shown as (39), the asymptotic stability for the proposed backstepping control is given, which proves the closed-loop system is stable and the tracking convergence can be achieved.

V. Experiments

A. Experimental Setup

Five healthy subjects (male, 25 ± 3 years old, 172 ± 4 cm, 65 ± 10.2 kg) were recruited in the experiments in this article with written consents and all the experimental protocols were admitted by the Institutional Review Board in the Faculty of Engineering, Kagawa University (Ref. No. 01-011).

In this article, a bilateral curl movement of elbow FE in the sagittal plane was selected as the bilateral rehabilitation training

Authorized licensed use limited to: NANKAI UNIVERSITY. Downloaded on April 19,2023 at 02:19:00 UTC from IEEE Xplore. Restrictions apply.

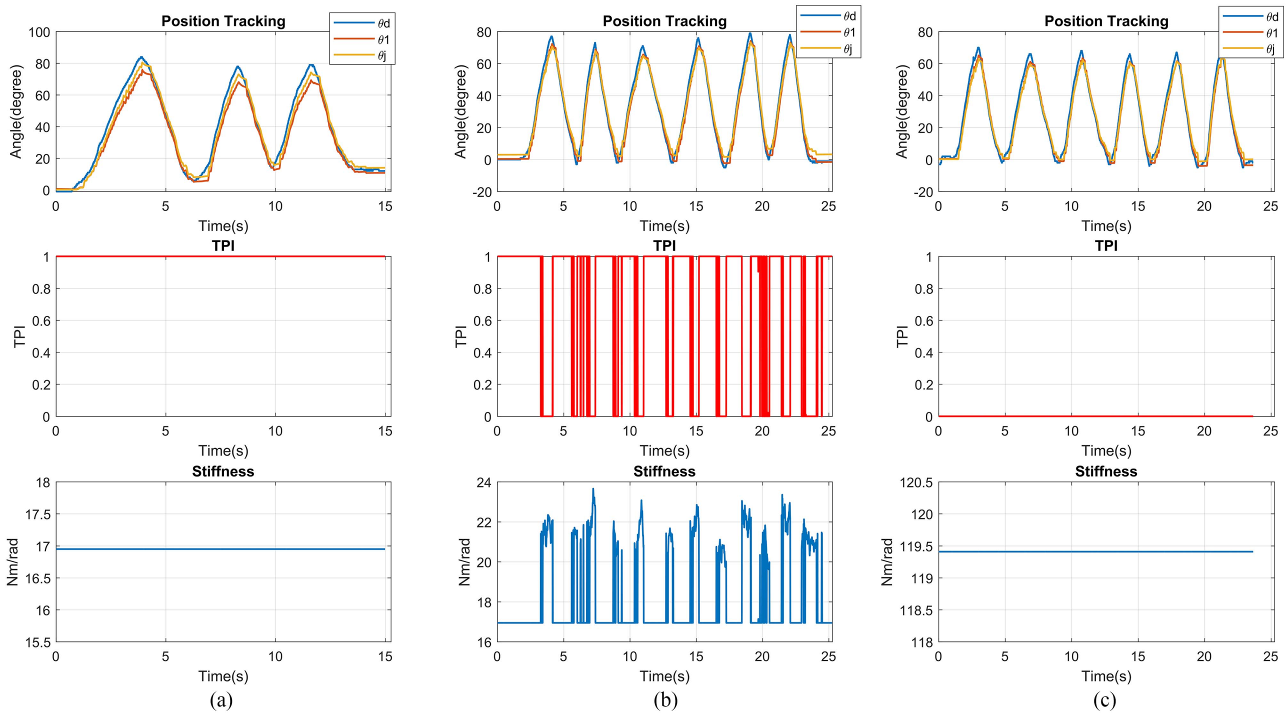

Fig. 8. Comparison results in three different stiffness modes. (a) Patient-in-charge mode. (b) Patient-robot cooperation mode (c) Robot-in-charge mode. In the position tracking figures, the blue line represents the non-paretic limb (master side) trajectory, the orange line is main frame trajectory, and the red line refer to the robot-assisted affected limb (slave side) trajectory.

task to evaluate the proposed task performance-based variable stiffness control strategy. In this experiment, the subjects were instructed to perform the left nonparetic limb the voluntary curl movement of elbow FE. Meanwhile, the right affected limb wearing the PVSED will be asked to track the left side limb with the maximum patient voluntary participants. Three inertial measurement units (GY-25T tilt angle module) were implemented on the health side forearm, the output link of the PVSED, and on the mainframe of the PVSED, respectively, for calculating the tracking errors and the compliant deviation of PVSED. Furthermore, the EMG signals of the healthy side limb biceps and triceps will be collected during the bilateral curl movements for calculating the real-time reference stiffness. In other to evaluate the patient voluntary participants, a thin film contact force sensor was placed into the upper support frame to measure the contact force during elbow bilateral curl movements. The experimental setups were shown in Fig. 7.

B. Experimental Protocol

Total two sets of experiments were designed and carried out to reveal how the stiffness and assistance of PVSED could be regulated by the proposed control strategy. First, the comparison validation experiments of three stiffness modes were conducted as a demonstration to reveal the characteristics of control framework. The system will work in robot-in-charge mode, patient-robot cooperation mode, and patient-in-charge mode, by setting the different parameters of TPI. Then, to verify the influence of different training task intensities, the subjects will be instructed to lift a dumbbell (0, 1.5, 2.5 kg) during the elbow bilateral curl movement to simulate the different training task intensities. The control parameters used were $k_1 = 0.68$, $k_2 = 0.42$, $k_3 = 100$, $k_4 = 50$, correspond to system parameters set as $J_j = 0.53\ \mathrm{kgm}^2$, $B_j = 0.24$ Nm/rad, g = 9.81 m/s^2, $J_1 = 0.0052\ \mathrm{kgm}^2$, and $B_1 = 0.0021$ N·m/rad.

C. Experimental Results

1) Experiment 1: Comparison Validation Experiments of Three Different Stiffness Modes: To verify the characteristic of three stiffness control modes, the comparison validation experiments were carried out, which require the control system would only work in one stiffness mode at one experimental trial. Therefore, a demonstration was performed and its results were introduced as follows:

1) *Patient-in-Charge Mode*: In this experiment, the regions were set as $R_a = 50°$, $R_p = 100°$, to ensure the TPI $\rightarrow 1$ and the system will work in patient-in-charge mode. Due to the TPI $\rightarrow 1$, the stiffness will be kept to the minimum value ($\theta_2 = 0°$, $K = 16.95$ N·m/rad) shown as Fig. 8(a), and the average tracking error is 10.85 °. In this mode, subjects can only keep the high training performance by keeping high active voluntary of the affected side limb. If the ability was not enough to finish the training task, the deviation angle will be a relative maximum value compared with the other two modes.
2) *Patient-Robot Cooperation Mode*: In this experiment, by setting $R_a = 5°$, $R_a = 15°$ which is conforming to

Authorized licensed use limited to: NANKAI UNIVERSITY. Downloaded on April 19,2023 at 02:19:00 UTC from IEEE Xplore. Restrictions apply.

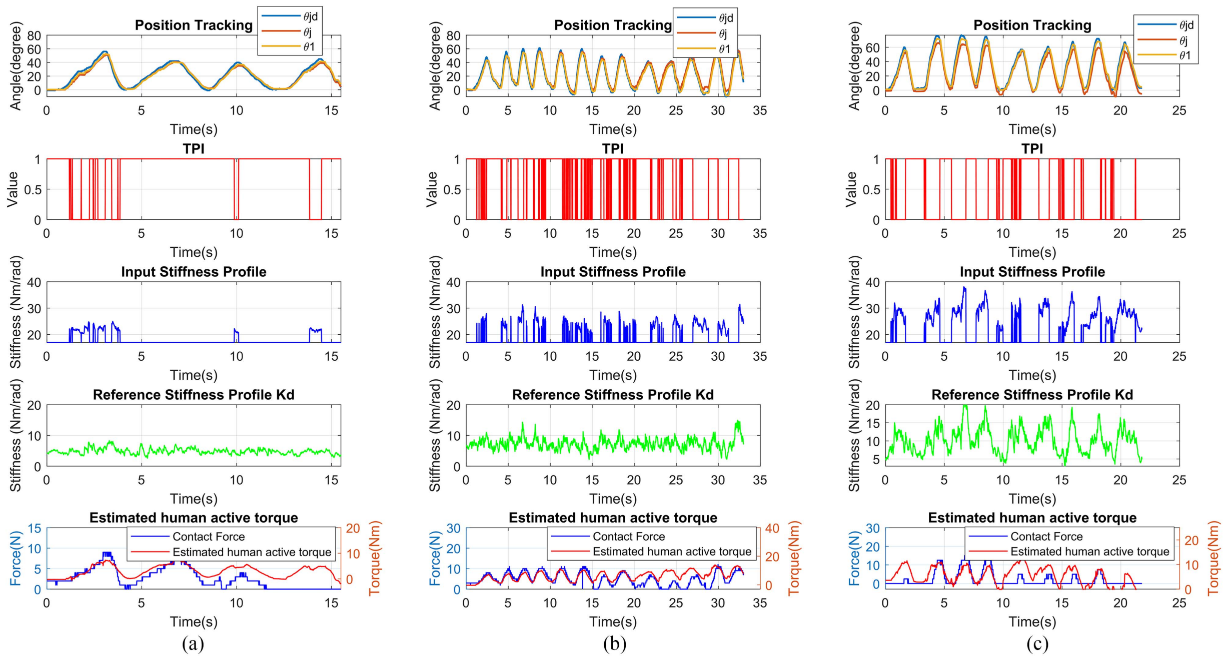

Fig. 9. Comparison results in three different task intensities of one subject. (a) Load 0 kg. (b) Load 1.5 kg. (c) Load 2.5 kg. In the position tracking figures, the blue line represents the nonparetic limb (master side) trajectory, the orange line is main frame trajectory, and the red line refer to the robot-assisted affected limb (slave side) trajectory.

real rehabilitation scenario, the patient-robot cooperation mode was activated. At the beginning of the experiment, the stiffness of the PVSED is a minimum value 16.95 N·m/rad. As we can see from Fig. 8(b), when the tracking error changed, the TPI smoothly transited within 1 to 0. Accordingly, the stiffness was simultaneously regulated within the minimum stiffness $\sigma_{\min}$ to the reference stiffness K_d in real time.

3) *Robot-in-Charge Mode*: The tracking error region was set at an absolute small value ($R_a = 0.1^\circ$, $R_p = 0.2^\circ$), so that TPI $\rightarrow 0$ to keep the system remaining the robot-in-charge mode. In this mode, the PVSED will play the dominant role to guide the affected side limb move according to the intact side limb by unaltered delivered the reference stiffness (set as the maximal stiffness of PVSED for obvious comparisons, $\theta_2 = 1440^\circ, K = 119.49$ N·m/rad) shown as Fig. 8(c). And the relatively minimum average tracking error is 3.92° among three modes.

2) Experiment 2: Comparison Validation Experiments of Different Training Intensities: To validate the feasibility and performance of the human-robot interaction of the proposed control strategy, all five subjects were instructed to perform the interaction experiments. For clarity in illustrating and analyzing the control performance, the results of one subject were shown in this part. All results of five subjects will be analyzed later.

1) ***0 Kg Load Condition:*** In the 0 kg load condition, which is the easiest difficulty for the patients like daily life condition, the sEMG-driven reference stiffness from the non-paretic side was kept as a relatively low value, shown as Fig. 9(a). Therefore, the stiffness regulation range was also relatively low consistent with the low training intensity. Due to the low level of sEMG signals, K_d was at a low level too, and the maximal slope of TPI was relatively low so the stiffness regulation speed was relatively lowest among the three load conditions. Accordingly, the impedance characteristic of PVSED was relatively low. Thus, the avenge contact force in this mode is 2.539 N which is also relatively low among the three modes.

2) *1.5 kg Load Condition:* When subjects performed the same elbow bilateral curl movement with 1.5 kg load, it can be clearly observed in Fig. 9(b) that the input stiffness level of the VSA was accordingly increasing due to the higher sEMG signals level. The higher stiffness amplitude renders the higher training difficulty and intensity, the higher impedance of PVSED, and the higher contact force (average force is 3.531 N). Moreover, the stiffness regulation speed also increased because of the faster TPI variation trend caused by higher K_d.

3) ***2.5Kg Load Condition:*** Similar as the characteristic of 1.5 kg load experiment, the reference stiffness K_d and regulation speed were further increased and accelerated by the higher sEMG amplitude level in 2.5 kg load condition, which also lead to the highest level of input stiffness and impedance characteristic among the three comparison experiments. As Fig. 9(c) shows when the tracking error exceeds R_a, the input stiffness of VSA rapidly increased to the reference stiffness K_d.

Benefiting from high stiffness level and fast stiffness regulation, the tracking error could be quickly eliminated, that subjects could be corrected to the desired trajectory position. And the average contact force is accordingly the highest among the three modes, which equals 4.635 N. Furthermore, the increasing trend

Authorized licensed use limited to: NANKAI UNIVERSITY. Downloaded on April 19,2023 at 02:19:00 UTC from IEEE Xplore. Restrictions apply.

TABLE I
PERFORMANCE OF FIVE SUBJECTS IN DIFFERENT LOADS

Subject	Load: 0kg				Load: 1.5kg				Load: 2.5kg			
	Average Deviation (deg)	Average K_d (Nm/rad)	Average K^{TPI} (Nm/rad)	Average Force (N)	Average Deviation (deg)	Average K_d (Nm/rad)	Average K^{TPI} (Nm/rad)	Average Force (N)	Average Deviation (deg)	Average K_d (Nm/rad)	Average K^{TPI} (Nm/rad)	Average Force (N)
Subject1	4.889	4.670	19.048	0.962	1.109	7.648	19.230	5.986	3.242	9.264	21.828	7.195
Subject2	6.719	4.725	19.608	2.213	-0.837	6.815	19.313	4.173	2.895	9.505	20.875	4.965
Subject3	2.863	5.161	18.843	4.551	-1.389	7.237	18.595	4.252	1.764	9.474	19.205	4.478
Subject4	6.756	5.236	20.131	2.353	-3.581	7.397	20.059	3.892	3.281	10.173	21.332	5.852
Subject5	1.107	4.856	17.852	2.539	-1.564	7.283	19.427	3.531	6.390	10.146	22.908	4.635

of the contact force from 0 kg load to 2.5 kg load can be observed, that might be caused by the increasing speed of TPI variation and faster stiffness regulation.

Under the same experimental condition, including the control parameters setting, the EMG signals collection preparation, and the PVSED mechanical setup, the other four subjects also successfully performed the same experiments in different loads (0, 1.5, and 2.5 kg), which verified the feasibility and repeatability of the proposed method (see Table I).

VI. Discussion

For the different injury levels of hemiplegia patients, the rehabilitation training task should be individual-specific, which requires the rehabilitation robotics can adaptively adjust the training task difficulty and intensity according to the patient-individuals [43]. Unsuitable tasks will let patients lose their concentration on the task and decline their participation, and lead to slacking during the training task. Therefore, suitable assistance should be delivered to the affected limb, which requires the rehabilitation robot can possess the capability of AAN control to promote patients' active participation. In addition, training safety is the other key metric of rehabilitation robotics, which always requires compliant pHRI characteristics. For the exoskeleton-type rehabilitation robotics, the torque sensors and contact force sensors are hard to implement due to the highly portable and position sliding problem, so the position-based control framework is expected for indirectly driven robotics. To adapt to the individual-specific condition of different injury levels, the rehabilitation training should have the ability to provide suitable assistance to patients according to their training performance. Furthermore, the stiffness transition should be smooth to avoid the damages caused by the discontinuous stiffness variation.

In this article, a training task performance-based stiffness control framework of a VSA-integrated robot was purposed to induce patients' maximum voluntary participation including three different stiffness modes. The TPI is designed by combining the training task accuracy and intensity to realize the autosmooth transition. With the employment of the TPI, the three different stiffness modes can be integrated into a single HLCL, and the transition among the three stiffness modes is smooth and stable which can avoid the discontinuous control input and stiffness variation. In the LLCL, the position-based bilateral impedance controller is utilized to plan the compliant position of the PVSED for providing human-like behavior patterns and task skills. Then, the desired compliant position can be tracked by a backstepping position controller.

Compared to the experimental trials of different training intensities, the measured contact force between the patient's forearm and arm support is shown in Fig. 9. Different from our previous study, in this article, the contact force is considered as the assess metric of the patient active voluntary level because the more assistance force transduction usually is achieved by the higher contact force. In the 0 kg load condition, from Fig. 9(a) 4–9.8 s and 10.2–13.8 s, the TPI is almost kept as 1 which means the high performance. The peak contact forces were decreasing from 9 N to 7 N and 4 N, which corresponds to the higher active participation. For this reason, it can be proof that the subjects must give more effort into the training to keep high task performance. Therefore, the purposed task performance quantitative factor TPI-based variable stiffness control framework was capable of inducing patient voluntary participation, demonstrated by the decreasing contact force. In addition, the contact force kept a low value when the TPI was 1 which can be also found in the high training intensity condition (2.5 kg load) as the Fig. 9(c) from 11 to 12.5 s. From this period, it can be observed that although the training task intensity was relatively high level, the stiffness still can be kept in a low level due to the high training task accuracy performance. If the training task performance is high, TPI $\rightarrow$ 1 and the system will work in the patient-in-charge mode, the stiffness would be kept at the minimum value to give a high allowance of motion range and minimum assistance to the patient. That means even the high ability subjects still need to give high participation into the task to keep the high tracking accuracy. This characteristic can be utilized for high-level ability patients or the patients in the high rehabilitation stage, which improves the adaptability of the specific individuals and task-oriented of the purposed control framework.

From Fig. 9, the average input stiffness values K^{TPI} are 17.852, 19.427, and 22.908 N·m/rad which corresponds to the reference stiffness K_d (4.856, 7.283, and 10.146 N·m/rad). Especially, from 0 to 10 s in the 2.5 kg load condition, it can be observed that, once the tracking error is too large and the training task performance is poor, the stiffness mode can be quickly switched and the stiffness level can be immediately changed by TPI, which can provide the higher assistance and lower allowance voluntary motion range to quickly correct tracking error. Therefore, the patient still can finish the training task with higher assistance. For the low-ability patients or some patients in the initial stage of rehabilitation, this quick correction control

Authorized licensed use limited to: NANKAI UNIVERSITY. Downloaded on April 19,2023 at 02:19:00 UTC from IEEE Xplore. Restrictions apply.

strategy is meaningful. The patients can regain their motor ability from the guidance from the non-paretic limb by repetitive bilateral movement training using the PVSED, which can prevent the patients from losing their confidence and promote their voluntary participation. Similarly, the experimental results of other four subjects also verified the abovediscussed phenomenon, which further showed the repeatability and effectiveness of the proposed control approach. Furthermore, from Table I, the experimental results of all five subjects indicated that the average input stiffness is related to both the average reference stiffness and the average deviation. This phenomenon verified that the assistant level is determined by both task performance and task intensity, which is consistent to the TPI design motivation and further valid the feasibility and the performance of the proposed control strategy.

VII. Conclusion

In this article, an sEMG-driven variable stiffness control with a novel training task quantitative factor TPI was proposed for upper limb elbow joint bilateral rehabilitation. First, the dynamics of the PVSED were analyzed for estimating the human active torque. Then, an sEMG-driven musculoskeletal model was utilized for calculating the real-time reference stiffness from nonparetic limbs as assistance guidance during the bilateral rehabilitation training. In the performance-based control law, a position-based impedance controller cascaded with a backstepping position controller was implemented as the LLCL for compliant position planning and tracking for bilateral limb coordination. Furthermore, the performance-based adaptive TPI was designed by considering both training accuracy and intensity to satisfy the individual-specific minimal assistance intervention for inducing maximal patient active participation to realize that the multiple stiffness modes can be integrated into a single high-level controller with a smooth and automatic transition. With the TPI regulation, the stiffness modes can be autosmoothly switched to address the potential stiffness discontinuous, hence guaranteeing safe human-robot interaction. Based on the purposed control frameworks, the demands of patients with different injury levels can be satisfied and the patient voluntary participant can be promoted for facilitating efficient upper limb rehabilitation. Future works will focus on the clinic application with hemiplegia patients to the actual training of patients.

References

[1] J. Wu, H. Cheng, J. Zhang, Z. Bai, and S. Cai, "The modulatory effects of bilateral arm training (BAT) on the brain in stroke patients: A systematic review," *Neurol. Sci.*, vol. 42, no. 2, pp. 501–511, 2021.

[2] P. M. Chen, P. W. H. Kwong, C. K. Y. Lai, and S. S. M. Ng, "Comparison of bilateral and unilateral upper limb training in people with stroke: A systematic review and meta-analysis," *PLoS One*, vol. 14, no. 5, pp. 1–21, 2019.

[3] R. K. Kim and N. Kang, "Bimanual coordination functions between paretic and nonparetic arms: A systematic review and meta-analysis," *J. Stroke Cerebrovascular Dis.*, vol. 29, no. 2, Feb. 2020, Art. no. 104544.

[4] D. Leonardis et al., "An EMG-controlled robotic hand exoskeleton for bilateral rehabilitation," *IEEE Trans. Haptics*, vol. 8, no. 2, pp. 140–151, Apr.–Jun. 2015.

[5] T. Chen, R. Casas, and P. S. Lum, "An elbow exoskeleton for upper limb rehabilitation with series elastic actuator and cable-driven differential," *IEEE Trans. Robot.*, vol. 35, no. 6, pp. 1464–1474, Dec. 2019.

[6] E. Trigili et al., "Design and experimental characterization of a shoulder-elbow exoskeleton with compliant joints for post-stroke rehabilitation," *IEEE/ASME Trans. Mechatronics*, vol. 24, no. 4, pp. 1485–1496, Aug. 2019.

[7] X. Cui, W. Chen, X. Jin, and S. K. Agrawal, "Design of a 7-DOF cable-driven arm exoskeleton (CAREX-7) and a controller for dexterous motion training or assistance," *IEEE/ASME Trans. Mechatronics*, vol. 22, no. 1, pp. 161–172, Feb. 2017.

[8] Q. Miao, M. Zhang, A. McDaid, Y. Peng, and S. Q. Xie, "A robot-assisted bilateral upper limb training strategy with subject-specific workspace: A pilot study," *Robot. Auton. Syst.*, vol. 124, 2020, Art. no. 103334.

[9] Q. Chen, B. Zi, Z. Sun, Y. Li, and Q. Xu, "Design and development of a new cable-driven parallel robot for waist rehabilitation," *IEEE/ASME Trans. Mechatronics*, vol. 24, no. 4, pp. 1497–1507, Aug. 2019.

[10] W. Meng, S. Q. Xie, Q. Liu, C. Z. Lu, and Q. Ai, "Robust iterative feedback tuning control of a compliant rehabilitation robot for repetitive ankle training," *IEEE/ASME Trans. Mechatronics*, vol. 22, no. 1, pp. 173–184, Feb. 2017.

[11] J. Narayan, B. Kalita, and S. K. Dwivedy, "Development of robot-based upper limb devices for rehabilitation purposes: A systematic review," *Augmented Hum. Res.*, vol. 6, no. 1. pp. 1–33, 2021.

[12] J. Bessler et al., "Safety assessment of rehabilitation robots: A review identifying safety skills and current knowledge gaps," *Front. Robot. AI*, vol. 8, no. 33, pp. 1–18, 2021.

[13] H. Yu, S. Huang, G. Chen, Y. Pan, and Z. Guo, "Human–robot interaction control of rehabilitation robots with series elastic actuators," *IEEE Trans. Robot.*, vol. 31, no. 5, pp. 1089–1100, Oct. 2015.

[14] S. Wolf et al., "Variable stiffness actuators: Review on design and components," *IEEE/ASME Trans. Mechatronics*, vol. 21, no. 5, pp. 2418–2430, Oct. 2016.

[15] B. Vanderborght, A. Albu-schaeffer, A. Bicchi, E. Burdet, and D. G. Caldwell, "Variable impedance actuators: A review," *Robot. Auton. Syst.*, vol. 61, no. 12, pp. 1601–1614, 2013.

[16] L. Liu, S. Leonhardt, and B. J. E. Misgeld, "Experimental validation of a torque-controlled variable stiffness actuator tuned by gain scheduling," *IEEE/ASME Trans. Mechatronics*, vol. 23, no. 5, pp. 2109–2120, Oct. 2018.

[17] V. Grosu, C. Rodriguez-Duerrero, S. Grosu, B. Vanderborght, and D. Lefeber, "Design of smart modular variable stiffness actuators for robotic-assistive devices," *IEEE/ASME Trans. Mechatronics,* vol. 22, no. 4, pp. 17777–11785, Aug. 2017.

[18] Z. Song and S. Guo, "Design process of exoskeleton rehabilitation device and implementation of bilateral upper limb motor movement," *J. Med. Biol. Eng.*, vol. 32, no. 5, pp. 323–330, 2012.

[19] S. Zhang et al., "Integrating compliant actuator and torque limiter mechanism for safe home-based upper-limb rehabilitation device design," *J. Med. Biol. Eng.*, vol. 37, no. 3, pp. 357–364, 2017.

[20] Z. Yang, S. Guo, Y. Liu, H. Hirata, and T. Tamiya, "An intention-based online bilateral training system for upper limb motor rehabilitation," *Microsyst. Technol.*, vol. 27, no. 1, pp. 211–222, 2020.

[21] S. Zhang, Q. Fu, S. Guo, and Y. Fu, "Coordinative motion-based bilateral rehabilitation training system with exoskeleton and haptic devices for biomedical application," *Micromachines*, vol. 10, no. 1, p. 8, 2018.

[22] Y. Liu, S. Guo, Z. Yang, and H. Hirata, and T. Tamiya, "A home-based bilateral rehabilitation system with sEMG-based real-time variable stiffness," *IEEE J. Biomed. Health Inform.*, vol. 25, no. 5, pp. 1529–1541, May 2021.

[23] Y. Liu, S. Guo, H. Hirata, H. Ishihara, and T. Tamiya, "Development of a powered variable-stiffness exoskeleton device for elbow rehabilitation," *Biomed. Microdevices*, vol. 20, no. 3, pp. 1–13, 2018.

[24] T. Proietti and V. Crocher, A. Roby-Brami, and N. Jarrassé, "Upper-limb robotic exoskeletons for neurorehabilitation: A review on control strategies," *IEEE Rev. Biomed. Eng.*, vol. 9, pp. 4–14, 2016.

[25] S. F. Atashzar, J. Carriere, and M. Tavakoli, "Review: How can intelligent robots and smart mechatronic modules facilitate remote assessment, assistance, and rehabilitation for isolated adults with neuro-musculoskeletal conditions?," *Front. Robot. AI*, vol. 8, Apr. 2021, Art. no. 610529.

[26] C. K. Thompson., D. B. den Ouden, B. Bonakdarpour, K. Garibaldi, and T. B. Parrish, "Neural plasticity and treatment-induced recovery of sentence processing in agrammatism," *Neuropsychologia*, vol. 48, no. 11, pp. 3211–3227, 2010.

[27] Q. Ai, Z. Liu, W. Meng, Q. Liu, and S. Q. Xie, "Machine learning in robot assisted upper limb rehabilitation: A focused review," *IEEE Trans. Cogn. Develop. Syst.*, early access, Jul. 19, 2021, doi: 10.1109/TCDS.2021.3098350.

Authorized licensed use limited to: NANKAI UNIVERSITY. Downloaded on April 19,2023 at 02:19:00 UTC from IEEE Xplore. Restrictions apply.

[28] A. U. Pehlivan, D. P. Losey, and M. K. Omalley, “Minimal assist-as-needed controller for upper limb robotic rehabilitation,” *IEEE Trans. Robot.*, vol. 32, no. 1, pp. 113–124, Feb. 2016.

[29] H. J. Asl, M. Yamashita, T. Narikiyo, and M. Kawanishi, “Field-based assist-as-needed control schemes for rehabilitation robots,” *IEEE/ASME Trans. Mechatronics*, vol. 25, no. 4, pp. 2100–2111, Aug. 2020.

[30] T. Teramae, T. Noda, and J. Morimoto, “EMG-based model predictive control for physical human-robot interaction: Application for assist-as-needed control,” *IEEE Robot. Autom. Lett.*, vol. 3, no. 1, pp. 210–217, Jan. 2018.

[31] L. Luo, L. Peng, C. Wang, and Z. Hou, “A greedy Assist-as-needed controller for upper limb rehabilitation,” *IEEE Trans. Neural Netw. Learn. Syst.*, vol. 30, no. 11, pp. 3433–3443, Nov. 2019.

[32] S. Y. Mounis and N. Z. Azlan, “Assist-as-needed control strategies for upper limb rehabilitation therapy : A review,” *Jurnal Mekanikal,* vol. 42, no. 1, pp. 57–74, 2019.

[33] L. Liu, M. Lüken, S. Leonhardt, and B. J. E. Misgeld, “EMG-driven model-based knee torque estimation on a variable impedance actuator orthosis,” in *Proc. IEEE Int. Conf. Cyborg Bionic Syst.*, 2017, pp. 262–267, doi: 10.1109/CBS.2017.

[34] L. Liu, S. Leonhardt, and B. J. E. Misgeld, “Impedance-controlled variable stiffness actuator for lower limb robot applications,” *IEEE Trans. Automat. Sci. Eng.*, vol. 17, no. 2, pp. 991–1004, Apr. 2020.

[35] E. Sariyildiz and K. Ohnishi, “Stability and robustness of disturbance-observer-based motion control systems,” *IEEE Trans. Ind. Electron.*, vol. 62, no. 1, pp. 414–422, Jan. 2015.

[36] K. Gui, H. Liu, and D. Zhang, “Toward multimodal human-robot interaction to enhance active participation of users in gait rehabilitation,” *IEEE Trans. Neural Syst. Rehabil. Eng.*, vol. 25, no. 11, pp. 2054–2066, Nov. 2017.

[37] Q. Wu, X. Wang, B. Chen, and H. Wu, “Development of a minimal-intervention-based admittance control strategy for upper extremity rehabilitation exoskeleton,” *IEEE Trans. Syst., Man, Cybern., Syst.*, vol. 48, no. 6, pp. 1005–1016, Jun. 2018.

[38] J. Zhang and C. C. Cheah, “Passivity and stability of human-robot interaction control for upper-limb rehabilitation robots,” *IEEE Trans. Robot.*, vol. 31, no. 2, pp. 233–245, Apr. 2015.

[39] X. Li, Y. Pan, G. Chen, and H. Yu, “Adaptive human-robot interaction control for robots driven by series elastic actuators,” *IEEE Trans. Robot.*, vol. 33, no. 1, pp. 169–182, Feb. 2017.

[40] X. Li, Y. Pan, G. Chen, and H. Yu, “Multi-modal control scheme for rehabilitation robotic exoskeletons,” *Int. J. Robot. Res.*, vol. 36, no. 5–7, pp. 759–777, 2017.

[41] J. Xu et al., “A multi-mode rehabilitation robot with magnetorheological actuators based on human motion intention estimation,” *IEEE Trans. Neural Syst. Rehabil. Eng.*, vol. 27, no. 10, pp. 2216–2228, Oct. 2019.

[42] X. Li, Q. Yang, and R. Song, “Performance-based hybrid control of a cable-driven upper-limb rehabilitation robot,” *IEEE Trans. Biomed. Eng.*, vol. 68, no. 4, pp. 1351–1359, Apr. 2021.

[43] N. Naghavi, A. Akbarzadeh, S. M. Tahamipour-z, and I. Kardan, “Assist-As-Needed control of a hip exoskeleton based on a novel strength index,” *Robot. Auton. Syst.*, vol. 134, 2020, Art. no. 103667.

[44] B. K. Dinh, M. Xiloyannis, C. W. Antuvan, L. Cappello, and L. Masia, “Hierarchical cascade controller for assistance modulation in a soft wearable arm exoskeleton,” *IEEE Robot. Automat. Lett.,* vol. 2, no. 3, pp. 1786–1793, Jul. 2017.

[45] P. Bujalski et al., “A Monte Carlo analysis of muscle force estimation sensitivity to muscle-tendon properties using a hill-based muscle model,” *J. Biomech.*, vol. 79, pp. 67–77, 2018, doi: 10.1016/j.jbiomech.2018.07.045.

Ziyi Yang (Student Member, IEEE) received the M.S. degree in intelligent mechanical systems engineering in 2021 from Kagawa University, Takamatsu, Japan, where he is currently working toward the Ph.D. degree with Human-assistive Robotics, Kagawa University, Japan.

He has authored or coauthored more than 11 refereed journal and conference papers. His research interests include rehabilitation robotics, intelligent control theory and application, variable stiffness actuator, biosignals processing, human-robot interaction, and telerehabilitation systems.

Shuxiang Guo (Fellow, IEEE) received the Ph.D. degree in mechanoinformatics and systems from Nagoya University, Nagoya, Japan, in 1995.

He is currently a Chair Professor with the Beijing Institute of Technology, Beijing, China. His current research includes biomimetic underwater robots, minimal invasive surgery robot systems, and rehabilitation robotics.

Dr. Guo is an Editor-in-Chief for the *International Journal of Mechatronics and Automation.*

Yi Liu (Member, IEEE) received the Ph.D. degree in human-assistive robotics from Kagawa University, Takamatsu, Japan, 2021.

He is currently a Researcher of the National Rehabilitation Center for Persons with Disabilities, Tokorozawa, Japan. His research interests include the design of rehabilitation robots, variable stiffness actuator, bio-signals processing, human-robot interaction, and telerehabilitation systems.

Masahiko Kawanishi received the B.S. degree from the Faculty of Medicine, Kagawa Medical University, Takamatsu, Japan, in 1993.

He is currently a Lecturer with the Faculty of Medicine, Kagawa University. He has authored or coauthored more than 80 refereed journal articles and conference papers. His current research interests include the surgical techniques of neurosurgical operations and intravascular surgery systems.

Hideyuki Hirata received the Ph.D. degree in mechanical engineering from Tokyo Institute of Technology, Tokyo, Japan, in 1992.

He is currently Professor with the Faculty of Engineering and Design, Kagawa University, Takamatsu Japan. He has authored or coauthored more than 40 refereed journal and conference papers. His current research includes material strength, material design, and microdevices based on computer simulation technology.

Authorized licensed use limited to: NANKAI UNIVERSITY. Downloaded on April 19,2023 at 02:19:00 UTC from IEEE Xplore. Restrictions apply.